La$_4$Cu$_3$MoO$_{12}$: A Novel Cuprate with Unusual Magnetism

Douglas A. Vander Griend,[†] **Sophie Boudin,**[†] **Vincent Caignaert,**[†]
Kenneth R. Poeppelmeier,[*,†] **Yanguo Wang,**[‡] **Vinayak P. Dravid,**[‡] **Masaki Azuma,**[§]
Mikio Takano,[§] **Zhongbo Hu,**[⊥] **and James D. Jorgensen**[⊥]

*Contribution from the Department of Chemistry, Department of Materials Science and Engineering, and
Science and Technology Center for Superconductivity, Northwestern University, 2145 Sheridan Road,
Evanston, Illinois 60208-3113, Institute for Chemical Research, Kyoto University, Uji,
Kyoto-Fu 611, Japan, and Argonne National Laboratory, 9700 South Cass Avenue,
Argonne, Illinois 60439*

Received December 28, 1998

Abstract: La$_4$Cu$_3$MoO$_{12}$ is a new (ABO$_3$)$_{n=4}$ cuprate with mixed *B*-cations in a ratio of 1:3. When synthesized at ambient pressure, the structure is not perovskite as expected but rather a homeotype of YAlO$_3$, a rare-earth hexagonal phase. While the *P*6$_3$/*mmc* and *Pmnm* space groups can be used to model average structures which appear in quenched samples; powder, electron, and neutron diffraction data all confirm that a slow-cooled sample crystallizes in the monoclinic space group, *P*112$_1$/*m*. The copper and molybdenum are coordinated by oxygen in corner-sharing trigonal bipyramids that are sandwiched between layers of lanthanum cations. In the *B*-cation layer, the copper cations order into a kagomé-like lattice of triangular clusters. The magnetism has been measured from 2 to 800 K and is highly influenced by the geometric arrangement of the Cu^{II} cations. An antiferromagnetic transition occurs at 5 K, but the sample does not reach a purely paramagnetic state until 460 K.

Introduction

Cation arrangement within a structure is a primary focus in the development of new high-temperature superconductors (HTSCs) and related materials. Both the nature of the mixed cations and the ratio can have a radical effect on the inner architecture of solids. Double perovskite structures in which half of the *B*-cations are copper (A$_2$BCuO$_6$) adopt one of three arrangements: random, rock salt, and layered.[1] The layered configuration is the most rare and the most interesting because it possesses the cuprate planes essential to high-temperature superconductivity. The same *B*-cation stoichiometry has also been incorporated into quadruple perovskite structures which are layered and oxygen deficient.[2] The copper cations are five- not six-coordinate, and the cuprate planes are quite flat. Related phases of quintuple and sextuple perovskite, which contain even less copper, can be also be formed with layered structures.[3] A common characteristic of all these oxides is the orthogonal connectivity of the *B*-cations. In fact, all known HTSC's possess square cuprate lattices parallel to the superconductive current. This configuration dominates the normal state magnetism

because antiferromagnetic coupling of all of the Cu^{II} spins via Cu–O–Cu exchange can occur facilely. Understanding how stoichiometry relates to structure and how structure relates to properties is paramount to designing better materials. It is with this in mind that we now introduce a detailed examination of the unusual structure and magnetism of an ABO$_3$-type compound with a *B*-cation ratio of 3:1, La$_4$Cu$_3$MoO$_{12}$.

The title phase was synthesized under ambient pressure and was recently shown to be a polymorphic precursor to a layered perovskite phase that forms under high pressure in a cubic anvil-type apparatus.[4] The ambient pressure phase is fascinating in its own right, however, because it combines striking similarities and differences with previously studied cuprate systems. It contains familiar species: large lanthanum cations, small copper and molybdenum cations, and oxygen anions in the ratios of 1:1:3 as in perovskite, yet forms a phase with unusually low coordination of the constituents at ambient pressure. Molybdenum is comparable in size with copper, and its presence in a high oxidation state is critical. Since the average charge for cations in ABO$_3$ compounds is 3+, each Mo^{VI} offsets the charge of three divalent coppers. Furthermore, the 1:3 ratio of *B*-cations facilitates the formation of a geometrically frustrated magnetic lattice of Cu^{II} cations (d^9) that closely resembles a kagomé lattice.[5] The spins of the Cu^{II} cations can couple antiferromagnetically along the Cu–O–Cu bridges, but now the cuprate lattice is based on triangles rather than squares. These features provide an opportunity to compare and contrast structure–property relationships and to study the unique solid-state chemistry of copper.

* To whom correspondence should be addressed.

† Department of Chemistry and Science and Technology Center for Superconductivity, Northwestern University.

‡ Department of Materials Science and Engineering and Science and Technology Center for Superconductivity, Northwestern University.

§ Kyoto University.

⊥ Argonne National Laboratory.

(1) Anderson, M. T.; Greenwood, K. B.; Taylor, G. A.; Poeppelmeier, K. R. *Prog. Solid St. Chem.* **1993**, *22*, 197–233.

(2) Anderson, M. T., Poeppelmeier, K. R., Zhang, J.-P., Fan, H.-J., Marks, L. D. *Chem. Mater.* **1993**, *4*, 1305–1313.

(3) (a) Otzschi, K. D.; Poeppelmeier, K. R.; Salvador, P. A.; Mason, T. O.; Sinkler, W.; Zhang, H.; Marks, L. D. *Phys. C.* **1997**, 837–838. (b) Zhu, W. J.; Huang, Y. Z.; Ning, T. S.; Zhao, Z. X. *Mater. Res. Bull.* **1995**, 30, 243–246. (c) Otzschi, K. D.; Poeppelmeier, K. R.; Salvador, P. A.; Mason, T. O.; Zhang, H.; Marks, L. D. *J. Am. Chem. Soc.* **1996**, *118*, 8951–8952.

(4) Vander Griend, D. A.; Poeppelmeier, K. R.; Boudin, S.; Toganoh, H.; Azuma, M.; Takano, M. *J. Am. Chem. Soc.* **1998**, *120*, 11518–11519.

(5) Broholm, C.; Aeppli, G.; Espinosa, G. P.; Copper, A. S. *Phys. Rev. Lett.* **1990**, *65*, 3173–3176.

Experimental Section

Synthesis. Polycrystalline samples of $La_4Cu_3MoO_{12}$ were prepared at ambient pressure by solid-state reaction of stoichiometric amounts of $LaO_{1.5}$, CuO, and MoO_3. Powders were ground, pressed into pellets (2 metric ton·cm^{-2}), and fired at 1025 °C in air for 4 days with two intermittent grindings. Sacrificial pellets were used to avoid reaction with the alumina crucible. Two $La_4Cu_3MoO_{12}$ samples were prepared: the first sample was quenched in air, and the second was slow-cooled at 36 °C·h^{-1}.

X-ray Diffraction. Powder X-ray diffraction (PXD) data for both samples were collected every 0.02° for 3° < 2θ < 120° on a Rigaku RINT 2000 diffractometer. The refinement of the PXD data for the slow-cooled sample was performed using the Rietveld analysis program FULLPROF.[6]

Thermogravimetric Analysis. Thermogravimetric analysis (TGA) was conducted on the quenched sample in a mixture of 7% hydrogen and 93% nitrogen at 600 °C.

Electron Diffraction. Both samples were ground in agate mortars and dispersed in acetone. Thin fragments of the crystallite were collected on a holey carbon film supported on a copper grid. Transmission electron microscopy (TEM) observation was carried out at 200 kV using a Hitachi-8100 electron microscope. Large-angle tilt electron diffraction (LATED) and convergent beam electron diffraction (CBED) along different zone axes were used to determine the crystal symmetry and the space group of the detected phases. Also, an HF-2000 electron microscope with cooled field emission gun was used to perform energy dispersive spectroscopy (EDS) on both samples.

Neutron Diffraction. The intense pulsed neutron source (IPNS) and special environment powder diffractometer at Argonne National Laboratory were used to collect time-of-flight data on the slow-cooled sample only. Approximately 5 g of the sample was encapsulated in a thin-walled vanadium can, and data were collected for 1 h at ambient temperature and pressure. Data from the detector bank at 144.8° 2θ were used in the final Rietveld refinement. Reflections between 0.5 and 4.0 Å were used in the refinement. The coherent scattering lengths for La, Cu, Mo, and O were taken to be 8.27, 7.718, 6.96, and 5.805 fm, respectively.[7] The neutron diffraction data were corrected for absorption, and there was no evidence for a preferred orientation. Rietveld refinement of the neutron data was carried out using the general structure analysis system (GSAS).[8]

Magnetic Susceptibility. Susceptibility measurements for the quenched sample were performed on a Quantum Design MPMS SQUID magnetometer from 5 to 350 K in an external field of 1 T. The slow-cooled sample was measured in a Quantum Design MPMS XL SQUID from 5 to 400 K and then from 300 to 800 K in a Quantum Design MPMS SQUID with sample space oven accessory. Finally, the susceptibility of this sample was measured on heating and cooling from 2 to 20 K. For each measurement, the remnant field was measured with a lead sample and the external field adjusted to offset it. All susceptibilities are reported as molar susceptibilities per copper ion.

Results

No binary oxides were detected in the PXD data for either sample, and the TGA result (4.64% weight loss) verifies the formula $La_4Cu_3MoO_{12}$. The intense PXD reflections can be indexed on a hexagonal cell with $a = 3.95$ Å and $c = 11.00$ Å. The details of the Rietveld refinement of the PXD data based on the hexagonal cell have been reported previously.[4] The extinction condition, *hhl* ($l = 2n + 1$) indicates that $P6_3/mmc$ is the appropriate space group, so the structure of $La_4Cu_3MoO_{12}$ synthesized at ambient pressure could be isotypic with such hexagonal structures as $YAlO_3$, $InFeO_3$, and $InMnO_3$.[9-11] This
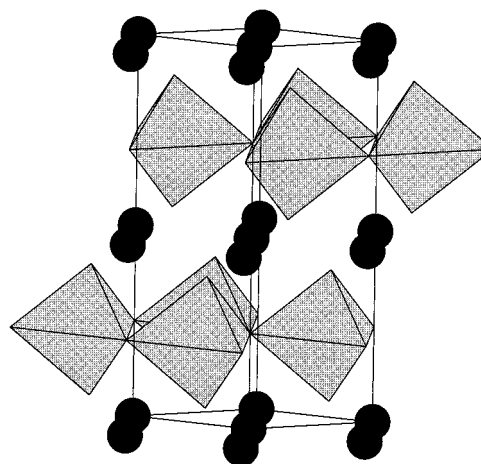

Figure 1. Perspective view of the $YAlO_3$ structure. Dark circles are yttrium, and shaded trigonal bipyramids are aluminum.
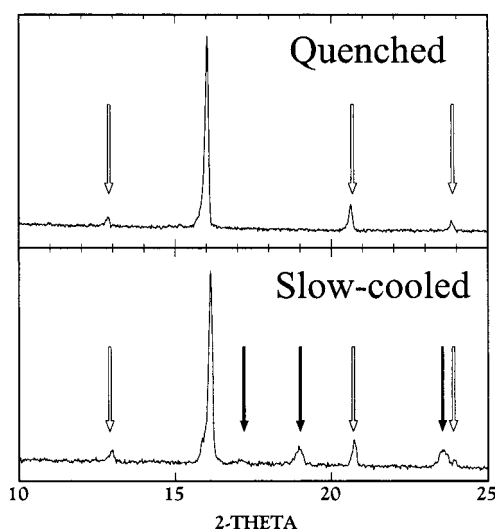

Figure 2. Enlarged view of PXD patterns of the quenched and slow-cooled samples.

ABO_3 structure type consists of layers of corner-sharing $BO_{3/3+2}$ trigonal bipyramids sandwiched between layers of *A*-cation (Figure 1). The effective coordination of the *A*-site can be either 6 ($InFeO_3$ and $InMnO_3$) or 6 + 2 ($YAlO_3$). Initial refinement used the atomic coordinates of $YAlO_3$ as a starting point and yielded decent agreement between the experimental and calculated patterns, but the thermal ellipsoids of the Cu/Mo and O in the [Cu/Mo–O]$_\infty$ planes are extremely broad within the plane for both samples. This result indicates that there are large deviations in the locations of *B*-cations and suggests that the Cu and Mo cations order within a larger cell. Furthermore, the PXD data show several weak reflections that cannot be indexed on the aforementioned hexagonal cell. Two related sets of weak reflections can be observed with intensities that vary on the basis of thermal treatment (Figure 2). The first set is present in both the quenched and slow-cooled samples and can be indexed with a hexagonal supercell of $a' = 2a$ and $c' = c$ or an orthorhombic cell of $a' = a$, $b' = \sqrt{3}a$, and $c' = c$. The second set of reflections appears only in slow-cooled samples and can be indexed with an orthorhombic cell of $a' = 2a$, $b' = \sqrt{3}a$, and $c' = c$.

(6) Rodriguez-Carvajal, J. Fullprof version 3.1, ILL, France, January 1996.

(7) Dears, V. F. Chalk River Nuclear Laboratory, Internal Report AECL-8490, 1984.

(8) Larson, A.; Von Dreele, R. B. *The General Analysis System*; Los Alamos National Laboratory: Los Alamos, NM, 1985.

(9) Bertaut, E. F.; Mareschal, *C. R. Acad. Sci.* **1963**, *275*, 867−870.

(10) Giaquinta, D. M.; Davis, W. M.; zur Loye, H.-C. *Acta Crystallogr.* **1994**, *C50*, 5−7.

(11) Giaquinta, D. M.; zur Loye, H.-C. *J. Am. Chem. Soc.* **1993**, *114*, 10952−10953.
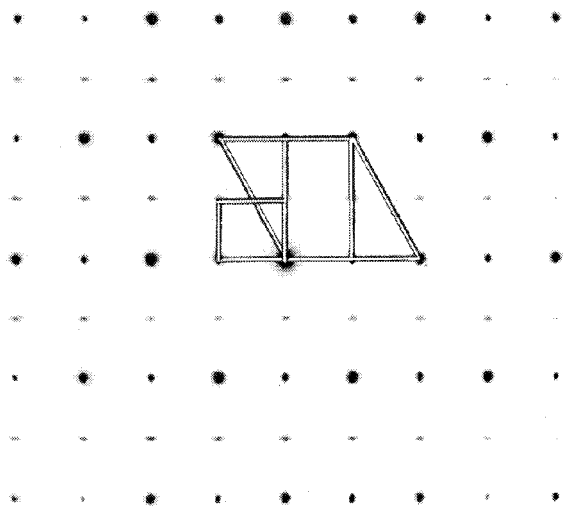
Figure 3. Reconstructed reciprocal planefrom the electron diffraction of phase 3. The basal plane of the monoclinic cell (small rectangle) is shown in contrast with the basal planes of the orthorhombic and hexagonal phases 1 and 2, respectively.

While two samples were prepared, three different phases with subtle differences in structure were identified using electron diffraction (ED): two in the quenched sample (phase 1 and phase 2) and one in the slow-cooled sample (phase 3). The chemical composition ratios of all three phases as measured by EDS correspond to the formula $La_4Cu_3MoO_{12}$. The supercells and symmetries of all three phases were determined with LATED and CBED. Details of the ED experiment can be found in the Supporting Information. Here we present only the essential crystallographic data for each phase.

Phase 1, from the quenched sample, crystallizes in $P6_3/mmc$ with measured parameters of approximately $a \cong 4$ Å and $c \cong 11$ Å. Phase 2, also from the quenched sample, crystallizes in $Pmnm$. $Pmnm$ is an orthorhombic subgroup of $Cmcm$, which in turn is a subgroup of the hexagonal space group $P6_3/mmc$. The lattice parameters are $a_o = a_h \cong 4$ Å, $b_o = \sqrt{3}a_h \cong 6.9$ Å, and $c_o = c_h \cong 11$ Å, where the subscripts h and o designate the hexagonal and orthorhombic cells, respectively. Finally, phase 3 is the only phase found in the slow-cooled sample and crystallizes in the $P112_1/m$ space group. Measured lattice parameters for this monoclinic phase are: $a_m = 2a_h \cong 8$ Å, $b_m = \sqrt{3}a_h \cong 6.9$ Å, $c_m = c_h \cong 11$ Å, and $\gamma = 90°$, where the subscript m designates the monoclinic cell. It is important to remember that, even though the cell is orthorhombic because $\gamma = 90°$, the symmetry is monoclinic because the mirror plane perpendicular to the a axis no longer exists. From this point forward in the paper, the hexagonal ($P6_3/mmc$), orthorhombic ($Pmnm$), and monoclinic ($P112_1/m$) phases will be referred to as 1, 2, and 3, respectively.

Figure 3 shows the reconstructed reciprocal [001] plane for 3 and the basal planes of the hexagonal and orthorhombic cells of 1 and 2. From this figure it is clear that 3 represents a superstructure of both 1 and 2. It possesses all the same atom connectivity, but the unit cell is larger and less symmetric. Consequently there are more independent atomic sites. We infer that the cations in the monoclinic cell are more ordered because the more slowly the sample is cooled the more intense the supercell reflections become (Figure 2). It is reasonable for the Mo^{VI} and Cu^{II} cations to sit on independent sites since their coordination requirements are so different. This also allows the highly charged Mo^{VI} cations to maximize the distance between each other.
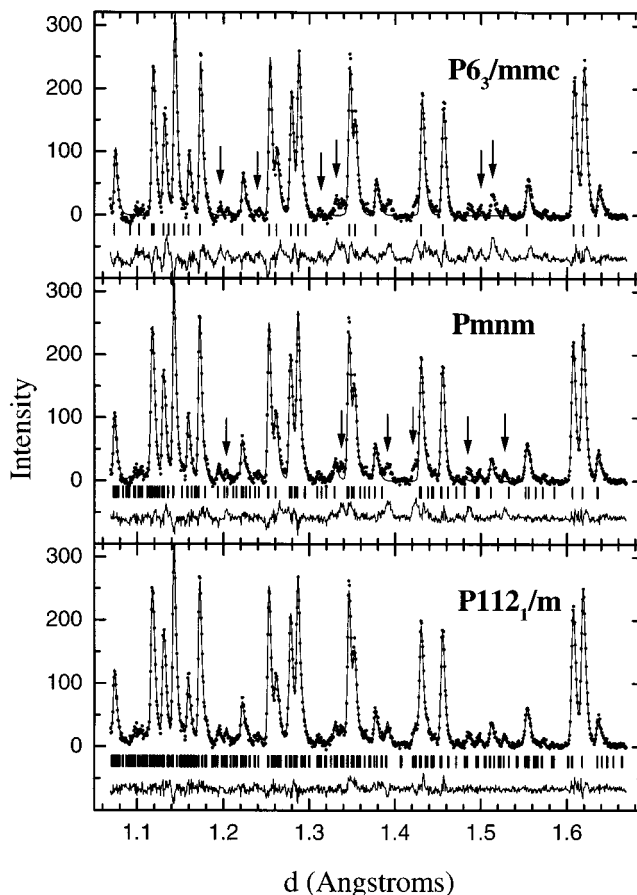

Figure 4. Enlarged view of observed and calculated powder neutron diffraction data for refinements in $P6_3/mmc$, $Pmnm$, and $P112_1/m$. Reflections which are not accounted for are indicated by arrows.

To investigate the B-cation ordering, time-of-flight neutron diffraction data were collected for the slow-cooled sample. According to both the X-ray and electron diffraction experiments only 3 is found in this sample. However, the neutron data were systematically refined in the space groups of all three phases for two reasons: to evaluate the nature of the disorder in 1 and 2 and to facilitate the convergence of the final solution. The specific results of the refinements in $P6_3/mmc$ and $Pmnm$ can be found in the Supporting Information.

The final structure from the refinement of the PXD data in the $P6_3/mmc$ space was used as a starting point for the Rietveld analysis of the neutron data. The measure of the goodness of fit, χ^2, could not be lowered past 2.58 since many weak reflections are not accounted for at all (Figure 4). The in-plane equatorial thermal parameters for the ions in the B-cation plane were about 4 times larger than expected, indicating that this solution is an average structure. Also, since the Cu^{II} and the Mo^{VI} occupy the same site, the bond valence calculations based on this refined structure are grossly incorrect.[12]

Next, the neutron data was refined in $Pmnm$, the space group of 2. The ideal atomic coordinates from the $P6_3/mmc$ model were translated to orthorhombic symmetry and used as the starting point for refinement. This orthorhombic cell is twice the volume as the hexagonal one, and the $Pmnm$ symmetry allows for atomic displacements along the b and c axes. It also has two independent crystallographic sites for the copper and molybdenum cations ((Cu1/Mo1) and (Cu2/Mo2)) as well as the coplanar oxygen (O3 and O4). Despite the lower symmetry,

(12) Brown, I. D.; Alternatt, D. *Acta Crystallogr., Sect B.* **1985**, *41*, 244−247.

Table 1. Possible Environments and Calculated Bond Valences for the Copper/Molybdenum Sites in the Monoclinic Structure[a]

cation site designation		bond valence for Mo^{VI} in subcell A	bond valence for Cu^{II} in subcell B
subcell A	subcell B		
O3 O4′ (Cu1/Mo1)	O3′ O4 (Cu1/Mo1)′	**5.73**	2.76
O3 O4 (Cu1/Mo1)	O3′ O4 (Cu1/Mo1)′	4.34	
O3 O4′ (Cu1/Mo1)	O3′ O4′ (Cu1/Mo1)′	4.34	
O3 O4 (Cu1/Mo1)	O3′ O4′ (Cu1/Mo1)′	2.95	
O3′ O4′ (Cu1/Mo1)	O3 O4 (Cu1/Mo1)′	**6.25**[b]	**1.72**[b]
O3′ O4 (Cu1/Mo1)	O3 O4 (Cu1/Mo1)′	4.86	
O3′ O4′ (Cu1/Mo1)	O3 O4′ (Cu1/Mo1)′	4.86	
O3′ O4 (Cu1/Mo1)	O3 O4′ (Cu1/Mo1)′	3.47	
O3 O4′ (Cu1/Mo1)′	O3′ O4 (Cu1/Mo1)	4.56	
O3 O4 (Cu1/Mo1)′	O3′ O4 (Cu1/Mo1)	3.87	
O3 O4′ (Cu1/Mo1)′	O3′ O4′ (Cu1/Mo1)	3.87	
O3 O4 (Cu1/Mo1)′	O3′ O4′ (Cu1/Mo1)	3.18	
O3′ O4′ (Cu1/Mo1)′	O3 O4 (Cu1/Mo1)	**6.50**	**1.59**
O3′ O4 (Cu1/Mo1)′	O3 O4 (Cu1/Mo1)	**5.81**	**2.35**
O3′ O4′ (Cu1/Mo1)′	O3 O4′ (Cu1/Mo1)	**5.81**	**2.35**
O3′ O4 (Cu1/Mo1)′	O3 O4′ (Cu1/Mo1)	5.12	
O3 (Cu2/Mo2)	O3′ (Cu2/Mo2)′	3.43	**1.72**[b]
O3′ (Cu2/Mo2)	O3 (Cu2/Mo2)′	3.18	**1.85**[b]
O3 (Cu2/Mo2)′	O3′ (Cu2/Mo2)	3.43	**1.72**[b]
O3′ (Cu2/Mo2)′	O3 (Cu2/Mo2)	3.18	**1.85**[b]

[a] The (Cu2/Mo2)−O4 distances are not shown because they are greater than 2.8 Å. Bold type indicates an acceptable valence sum. [b] Assignments that were used in the subsequent refinement.

the thermal factors of these atoms remain highly anisotropic. The thermal ellipsoids of the (Cu1/Mo1) and O3 atoms are elongated along the *b* axis, while those of the (Cu2/Mo2) and O4 atoms are elongated along the *a* axis. Placing half of the ions at each end of their respective thermal ellipsoids (splitting the sites) yields the optimal goodness of fit factors for this space group: $\chi^2 = 1.94$, $R_{F^2} = 7.3\%$. Compared to the refinement in $P6_3/mmc$, disorder of the atoms in the *B*-cation plane is now along one dimension rather than two. Figure 4 shows how more of the weak peaks are accounted for in the neutron data with this refinement in *Pmnm*.

The most complete refinement uses the monoclinic cell of 3 found in the ED study of the slow-cooled sample. The atomic positions from the refinement in *Pmnm* provide a starting point. A monoclinic supercell can be built up from two adjacent orthorhombic unit cells, arbitrarily referred to here as A and B, which double the original orthorhombic cell in the *a* direction. There are now four independent sites for three copper cations and one molybdenum cation which must be assigned. In the *Pmnm* refinement, the Cu1/Mo1 site is split in the *b* direction into two sites ((Cu1/Mo1) and (Cu1/Mo1)′) which then alternate in the subcells of the monoclinic cell. The (Cu1/Mo1) site can be in subcell A and the (Cu1/Mo1)′ site in subcell B or vice versa. The same situation exists for the splitting of the O3 site. The situation is different for the (Cu2/Mo2) and O4 sites however. The mirror plane that intersects these sites in the orthorhombic cell does not exist in the monoclinic cell, so either split site can be occupied in either subcell regardless of the other. Subcell A could contain either the (Cu2/Mo2) or the (Cu2/Mo2)′ site, and subcell B could simultaneously contain either the (Cu2/Mo2) or the (Cu2/Mo2)′ site. The same is true with regard to the O4 and O4′ sites. This leads to eight possible coordination environments for the (Cu/Mo1) and (Cu/Mo1)′ sites and two for the (Cu/Mo2) and (Cu/Mo2)′ sites. Bond valence (BV) calculations provide a convenient way to narrow down the number of options.[12] Such calculations can also help to determine which site molybdenum occupies. Table 1 shows all possible cation environments in the [Cu/Mo−O]$_\infty$ layers with a

BV calculation for Mo occupation. Only five possibilities yield reasonable results (shown in bold), and the BVs for the corresponding Cu occupation are calculated for these cases. Cu exclusively occupies the (Cu2/Mo2) and (Cu2/Mo2)′ sites, and since the (Cu1/Mo1)′−O3′ bond distance of 1.54 Å is too short for a Mo−O bond in a MoO$_5$ polyhedron, Mo must be located on the (Cu1/Mo1) site. The one configuration of metal cations (Mo, Cu1′, Cu2, Cu2′) and corresponding oxygen anions in the *B*-cation plane which satisfies BV theory provides a starting point for the Rietveld refinement in $P112_1/m$. The final stage takes into account over 5300 reflections and converges to the unit cell with dimensions $a = 7.9125(4)$ Å, $b = 6.8503(4)$ Å, $c = 11.0113(2)$ Å, and $\gamma = 90.027(7)°$ with agreement factors of $\chi^2 = 1.5$ and $R_{F^2} = 5.4\%$. The atomic positions of all the atoms can be found in the Supporting Information. This space group accounts for all the peaks in the neutron data (Figure 4), and all the thermal factors are convincingly isotropic. The BV calculations based on the refined positions confirm the accuracy of the structure: BV(La^{III}) = 3.08 and 3.16, BV(Mo^{VI}) = 5.86, and BV(Cu^{II}) = 1.70, 1.77, and 1.93.[12] Small discrepancies are expected because of the unusual coordination of the cations, especially copper. It is important to recognize that throughout the refinement the positions of the La cations did not change appreciably and their coordination remained 6 + 2. In the final structure, six La−O distances are between 2.43 and 2.51 Å and the two longer distances are 2.73 and 2.83 Å.

The magnetism of both the quenched and slow-cooled samples was experimentally identical over the temperature range 5−350 K (Figure 5). Below 5 K there is a nonhysteretic antiferromagnetic region detected down to 2 K (T_N = 5 K). Above this transition, the data can be described by the Curie−Weiss law. From 10 to around 250 K, the inverse molar paramagnetic susceptibility is linear and corresponds to 1.127 μ_B per copper ion. Above 250 K, the magnetic behavior begins to crossover to a high-temperature region with a Weiss constant of approximately −460 K. Even though the standard deviation of the value of the inverse susceptibility is large, it is clear that above 460 K the Curie constant approaches the limit of approximately 1.73μ_B. This corresponds to the theoretical paramagnetic state for spin-$^1/_2$ cations.

Discussion

La$_4$Cu$_3$MoO$_{12}$ is typical in stoichiometry but exceptional in structure. ABO$_3$-type compounds are well-classified on the basis of ionic radii and bond ionicities.[13] However, by introducing multiple *B*-cations, A$_n$B$_m$B′$_{n-m}$O$_{3n}$, the situation becomes qualitatively different especially for cases involving copper. Unusual *B*-cation ordering schemes in perovskite, particularly those that lead to layering, have been far from predictable.[1] The new phase reported in this paper represents a crossover within ABO$_3$-type compounds between the perovskite and rare-earth hexagonal structures. The analogous lanthanide phases, Ln$_4$Cu$_3$MoO$_{12}$ (Ln = Nd, Pr, Sm−Tm) have all been synthesized under similar conditions, but because lanthanum is the largest, the structure of the title phase is the most unprecedented.

One of the most astounding aspects of the title phase is that it forms at all. Lanthanum has never been found in a homeotype of the YAlO$_3$ structure; neither has any other lanthanide cation larger than europium. The Goldschmidt tolerance factor for the lanthanum analogue is 0.91.[14] With such a value, we expect

(13) Giaquinta, D. M.; zur Loye, H.-C. *Chem. Mater.* **1994**, *6*, 365−372.

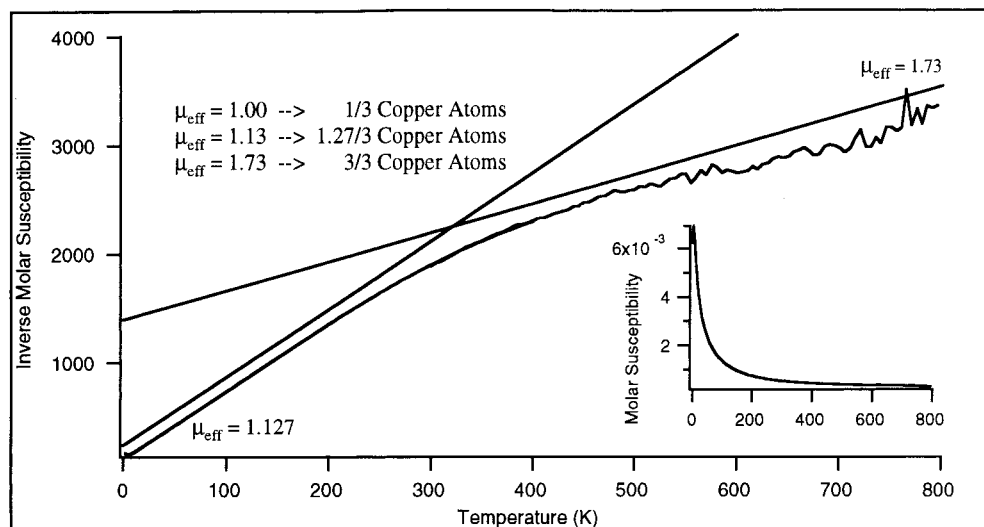(14) Goldschmidt, V. M. *Mater.-Nutrv. K.* **1926**, *2*, 117. Description of calculation is given in ref 4.

Figure 5. Inverse molar (per copper) magnetic susceptibility data for slow-cooled $La_4Cu_3MoO_{12}$ from 2 to 800 K. The straight lines show the slopes that correspond to $\mu_{eff} = 1.127\mu_B$ and $\mu_{eff} = 1.733\mu_B$. Inset shows the molar magnetic susceptibility data.

the stabilization of a perovskite structure, but the low-coordination, pseudohexagonal phase forms instead. $YAlO_3$ is a representative ABO_3-type compound which crystallizes in the $P6_3/mmc$ space group and even converts to perovskite above 1000° (the same is true of the rare earth manganates and ferrates).[15,16] In contrast, a cubic perovskite structure has never been made with the $La_4Cu_3MoO_{12}$ stoichiometry. A metastable, layered, monoclinic perovskite can be made under pressure, but the rare-earth pseudohexagonal structure is the thermodynamic product at ambient pressure. The contribution of copper to the structure can be inferred by comparing the title phase with the nickel analogue $La_4Ni_3MoO_{12}$.[17] Ni^{II} is about the same size as Cu^{II} but is not a Jahn−Teller ion, and $La_4Ni_3MoO_{12}$ forms a cubic perovskite at ambient pressure. Since La^{III} and Mo^{VI} can be incorporated facilely into such a structure, Cu^{II} must induce the formation of alternate structures. This is likely the result of the crystal chemistry associated with the copper coordination environment. Trigonal bipyramidal coordination is extremely rare for copper but is clearly preferred over the undistorted octahedral coordination of cubic perovskite and even the distorted octahedral coordination of the monoclinic layered perovskite.

　　$La_4Cu_3MoO_{12}$ is more closely related to $YAlO_3$ than to $InMO_3$ (M = Mn, Fe, Ga) because eight coordinating oxygens arrange in a flattened bicapped octahedron around the lanthanum. The difference between these two rare-earth compounds is the number of transition metals on the B site. Cu^{II} and Mo^{VI} are quite close in size, but it is not surprising that they order because they differ significantly in their charges. In the final monoclinic structure, the Mo^{VI} cations sit very close to ideal hexagonal positions, and the trigonal bipyramidal coordination with two short bond distances in the basal plane has been previously observed for Mo^{VI} in molybdophosphates.[18] The Cu cations however displace significantly from ideal hexagonal positions to form triangular clusters around the oxygens (Figure 6). Short Cu−O bond lengths within the cluster (1.7−2.0 Å) and long
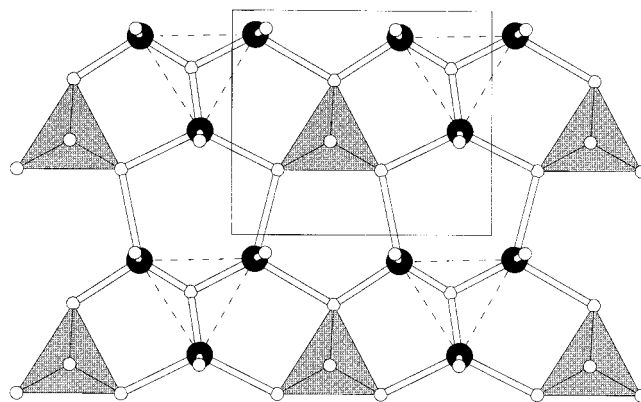
　　(15) Geller, S.; Wood, E. A. *Acta Crystallogr.* **1956**, *9*, 563−568.
　　(16) Wood, V. E.; Austin, A. E.; Collings, E. W.; Brog, K. C. *J. Phys. Chem. Solids* **1973**, *34*, 859−868.
　　(17) Torii, Y.; Matsumoto, H. *Yogyo-Kyokai-Shi* **1975**, *83*, 159−162.
　　(18) (a) Constentin, G.; Borel M. M.; LeClaire, A.; Grandin, A.; Raveau, B. *J. Solid State Chem.* **1991**, *95*, 168−175. (b) Guesdon, A.; Borel, M. M.; Leclaire, A.; Grandin, A.; Raveau, B. *J. Solid Sate. Chem.* **1994**, *109*, 145−151. (c) Borel M. M.; Guedson, A.; LeClaire, A.; Grandin, A.; Raveau, B. *Z. Anorg. All.* **1994**, *620*, 570−573.

Figure 6. Schematic view of the *B*-cation plane in the monoclinic structure of phase 3 ($P112_1/m$; $a = 7.9125(4)$ Å, $b = 6.8503(4)$ Å, $c = 11.0113(2)$ Å, $\gamma = 90.027(7)°$; $V = 596.84(5)$; $\chi^2 = 1.5$; $R_{F^2} = 5.4\%$). The basal plane of the unit cell is shown. Dotted lines between coppers (black circles) indicate the triangular clusters. Notice that the Mo cations (gray polyhedra) form an orthorhombic superlattice.

Cu−O bond lengths between clusters (≥ 2.5 Å) result in distorted trigonal bipyramidal coordination.

　　The subtle differences among the structures of 1, 2, and 3 arise from the arrangement and long-range order of the Cu and Mo cations. The refinements of the neutron data in both the $P6_3/mmc$ and $Pmnm$ space groups reveal not only that these solutions correspond to average structures but that they are average specifically because of disorder among the Cu^{II} and Mo^{VI}. Since the coordination requirements of these two cations differ considerably, the positions of the coplanar oxygens that coordinate to them also contribute to the supercell structure. A considerable amount of information on competing *B*-cation arrangements can be inferred from structural evidence along with the magnetic data, but these concepts will not be developed in this paper. As the *B*-cations order, the unit cell increases in size and decreases in symmetry from $P6_3/mmc$ to $Pmnm$ to $P112_1/m$. What does not change is the overall geometric symmetry of the lattice. In the fully ordered monoclinic structure, the ratio of the basal plane axes (b/a) remains 0.866 $= \sqrt{3}/2$. This is geometrically equivalent to the average hexagonal structure since $\sqrt{3}/2$ is the ratio of height to base in an equilateral triangle. This trend persists for the next five members of the series, $Ln_4Cu_3MoO_{12}$ (Ln = Nd, Pr, Sm−Gd).
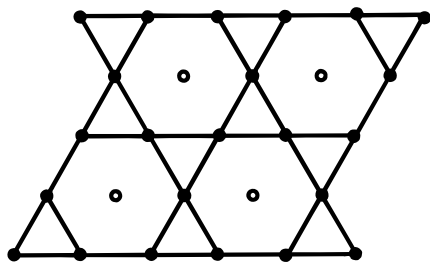
Figure 7. Schematic of a 2D kagomé lattice. Heteroatom positions (open circles) form a hexagonal superlattice.

Investigation continues on all the analogous phases to determine the details of their structures as well.

PXD, TGA, and EDS confirm the purity and stoichiometry of the title compound. Data from X-ray, electron, and neutron diffraction all verify the correctness of the final structure of 3. While small discrepancies in the exact atomic positions in the slow-cooled sample are plausible, the final χ^2 of 1.5 for the neutron data refinement in the monoclinic spacegroup is decidedly the lowest value achieved throughout all the refinements. To confirm this, the structure of 3 was refined again in $P112_1/m$, starting with the ideal hexagonal atomic positions except for the modified positions of the oxygen anions near the molybdenum site. It converged to the same structure as before.

The atomic structure of $La_4Cu_3MoO_{12}$ profoundly affects bulk properties such as magnetic susceptibility. Only Cu^{II} contributes to the spin magnetism of these phases, and in the fully ordered structure, the copper cations comprise a simple yet unique 2D lattice in the basal plane (Figure 6) which closely resembles a kagomé lattice because the magnetic species organize in a 2D hexagonal framework.[5] A kagomé lattice consists of corner-sharing triangular clusters of magnetic ions. The nonmagnetic ions sit $2a$ apart, forming a hexagonal superlattice with twice the dimensions of the original framework (Figure 7). In the title phase, however, three-member triangular clusters of Cu^{II} ions share corners and edges, and the nonmagnetic ions (Mo^{VI}) form an orthorhombic superlattice. The Mo^{VI} cations sit on sites that are $2a$ apart in the a direction but just $\sqrt{3}a$ apart in the b direction. In both cases spin pairing is geometrically frustrated because only two out of every three spins can pair antiferromagnetically. Perpendicular kagomé lattices can result in 3-D frustration, but this is not seen in the title phase.[19] Neighboring in-plane Cu^{II}'s (3.39–3.51 Å) interact strongly, but a distance of 6.1 Å between the B-cation planes renders the out-of-plane interactions relatively weak.

The bulk susceptibility can now be interpreted with respect to the cuprate lattice. The slope of the linear region of the inverse susceptibility from 15 to 250 K is equivalent to 0.635 spins per triangular copper cluster. This is slightly higher than the theoretical limit of $^1/_2$ spin per triangle that would result if two of the three Cu^{II} spins were paired. The difference may be attributed to a dynamic spin interaction within the triangular cluster clusters. The paramagnetic state is not achieved until 460 K owing to the strong interactions within the B-cation plane. Above this temperature, the slope approaches the upper theoretical limit of $1.73\mu_B$, which corresponds to three $^1/_2$ spins per triangular cluster.

The chemistry of the title phase is intimate with the atomic architecture. The striking differences in coordination and connectivity provide a new perspective for studying the contributions of copper to the structures and properties of materials. The presence of trigonally coordinated oxygen and copper creates an unusual magnetic lattice and must also promote an uncommon band structure since conventional band splittings for antiferromagnetic orthogonal orbital systems no longer apply. As synthesized, $La_4Cu_3MoO_{12}$ is an insulator, but it should afford the same opportunities for development of materials properties through doping and annealing that previous cuprate systems have. Introducing charge carriers via A-site or B-site doping would be a first step to modifying the physical properties. Copper would remain the focal element in p-doped analogues because doping will change either the average copper oxidation state or the coordination environment, and either of these changes will affect the stability of the title phase relative to the perovskite structure. Both 6-coordinate Cu^{III} and 4/5-coordinate Cu^{II} appear to facilitate the formation of the perovskite structure relative to 6-coordinate Cu^{II}. It may also be possible to stabilize $La_4Cu_3MoO_{12}$ as a perovskite in a thin film as was done with $YMnO_3$.[20]

Over the past decade, copper has owned a critical structural and electromagnetic role in the development of new materials. Despite intense effort to understand the structure–property relationships in cuprates, the search is not yet complete. The structure of $La_4Cu_3MoO_{12}$ represents a new multiple B-cation family in the $(ABO_3)_n$ system that provides a new motif for examining cuprate crystal chemistry. A homeotype of $YAlO_3$, it forms a monoclinic structure owing to the ordering of the copper and molybdenum in a slow-cooled sample. The familiar structure type and constitution facilitate the rational implementation of useful electronic and magnetic properties. Clearly the introduction of various B-cations dramatically affects the solid-state chemistry as evidenced by the magnetism of the insulating phase. Changing only the specific makeup of the B-cations has unveiled a whole new family of compounds in the familiar and bountiful system of cuprates.

Supporting Information Available: Detailed results and photos from the electron diffraction work, as well as tables listing detailed crystallographic data, atomic positions, bond lengths, and selected bond angles based on the Rietveld refinement of the neutron data for $La_4Cu_3MoO_{12}$ in all three different space groups (PDF). This material is available free of charge via the Internet at http://pubs.acs.org.

JA984436E

(19) Martinez, B.; Sandiumenge, F.; Rouco, A.; Labarta, A.; Rodriguez-Carvajal, J.; Tovar, M.; Causa, M. T.; Gali, S.; Obradors, X. *Phys. Rev. B.* **1992**, *46*, 10786–10792.

(20) Salvador, P. A.; Doan, T.-D.; Mercey, B.; Raveau, B. *Chem. Mater.* **1998**, *10*, 2592–2595.